Geometry Optimization of Magnetic Shunts in Power Transformers Based on a Particular Hybrid Finite-Element Boundary-Element Model and Sensitivity Analysis

Marina A. Tsili[1], *Student Member, IEEE*, Antonios G. Kladas[1], *Member, IEEE*, Pavlos S. Georgilakis[2], *Member, IEEE*, Athanassios T. Souflaris[3], and Dimitris G. Paparigas[3]

[1]Faculty of Electrical & Computer Engineering, National Technical University of Athens, GR-15780 Athens, Greece
[2]Department of Production Engineering and Management, Technical University of Crete, GR-73100 Chania, Greece
[3]Schneider Electric AE, GR-32011 Inofyta, Viotia, Greece

In this paper, the influence of magnetic shunt geometry on the transformer leakage field and short-circuit impedance is examined. The magnetic-field computation is conducted with the use of a particular hybrid finite-element method (FEM) boundary-element method (BEM) formulation, facilitating the parametric investigation of magnetic shunt effects through application of appropriate boundary conditions. A design sensitivity analysis for the optimization of the shunt geometry ensuring a desired change in short-circuit impedance and shunt losses has also been developed, in conjunction with the magnetic-field model.

***Index Terms*—Design optimization, finite-element (FEM) boundary-element (BEM) hybrid methods, sensitivity analysis, transformers.**

I. Introduction

NUMERICAL field-analysis techniques used in conjunction with optimization algorithms for the design optimization of magnetostatic devices are widely encountered in the technical literature and both the finite element method (FEM) [1], [2] and boundary element method (BEM) [3] have been employed for this purpose.

In cases where the difference between the actual (measured) and specified transformer short-circuit impedance value does not satisfy the contracted specifications or limitations imposed by international standards [4], design modifications should be implemented in order to meet the specifications. Appropriate magnetic shunts placed along the transformer tank walls can increase the magnetic leakage field and the winding leakage inductance. Experimental study of this kind of shields is carried out in [5], while in [6] and [7] the transformer tank shield geometry is optimized with the use of three-dimensional (3-D) FEM.

A method based on a particular FEM-BEM hybrid formulation has been developed in [8], presenting important advantages in power transformer parameter evaluation. In this paper, this method is extended to cases involving the shape optimization of power transformer magnetic shunts. The proposed method, which has been validated through local field measurements, is particularly suitable for use with optimization algorithms, as it reduces the total time needed for the magnetic field calculation during each iteration. The shape optimization is combined with the shunt power loss minimization, resulting to total cost reduction of the magnetic shielding.

Digital Object Identifier 10.1109/TMAG.2005.846075

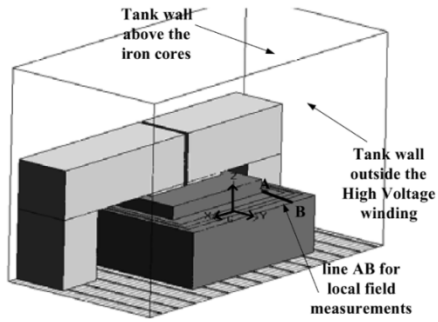

Fig. 1. Perspective view of the transformer one phase part modeled.

II. Transformer Modeling With Mixed FEM-BEM

For the transformer magnetic field simulation, a particular mixed FEM-BEM formulation was adopted [8]. Fig. 1 illustrates the three-dimensional one phase part model of the considered three-phase, wound core power transformers, consisting of the low-voltage (LV) and high-voltage (HV) winding of one phase as well as the iron cores that surround them. The model is divided in two regions.

1) The active part (FEM region), represented by a tetrahedral finite element mesh. A scalar potential formulation, necessitating no prior source field calculation [9] is used for the derivation of the magnetic scalar potential Φ in the mesh nodes.
2) The area between the active part and the tank walls (BEM region), represented by a triangular mesh of its boundaries.

This formulation is suitable for the transformer parameter evaluation and the considered optimization problem, as it enables

easier implementation of moving boundary of shield (along the tank walls) through BEM technique. Moreover, the choices of meshes for the transformer active part and shield are completely independent (a gradual mesh size change is necessary, in case of surrounding air discretization by FEM).

III. Geometry Optimization of Magnetic Shunt

A. Mathematical Formulation

The general mathematic form of the magnetic shunt geometry optimization consists in the minimization or maximization of an objective function $F(\mathbf{X}_i)$, where $\mathbf{X}_i$ is the vector of the design variables of the problem. In case of the magnetic shunt, the design variables comprise the geometrical parameters of the shunt, while the objective function is governed by the desired change in the transformer leakage field. The vector $\mathbf{X}_i$ is subject to constraints imposed by the transformer geometry (active part and tank dimensions).

B. Optimization Algorithms

The following optimization algorithms, [10], have been tested in case of magnetic shunt optimization.

1) Steepest Descent Method: The steepest descent is a gradient-based method, i.e., the search direction $\mathbf{S}_i$ for the optimal solution is constructed using the gradient of the objective function. The descent direction is obtained by reversing the gradient, according to

$$\mathbf{S}_i = -\nabla F(\mathbf{X}_i). \tag{1}$$

2) CG-FR Method: The conjugate gradient Fletcher–Reeves (CG-FR) method is a variation of the steepest descent method, where the search direction for the solution is given by

$$\mathbf{S}_i = -\nabla F(\mathbf{X}_i) + \frac{\nabla F(\mathbf{X}_i)^T \nabla F(\mathbf{X}_i)}{\nabla F(\mathbf{X}_{i-1})^T \nabla F(\mathbf{X}_{i-1})}. \tag{2}$$

3) DFP Method: The Davidon–Fletcher–Powell (DFP) method is a quasi-Newton, variable metric (VM), gradient-based method. In quasi-Newton methods, the history from all previous iterations is collected into a $n \times n$ matrix $[\mathbf{A}_i]$, called the metric, which is updated with each iteration and is used to establish the vector $\mathbf{S}_i$ as

$$\left.\begin{aligned} \mathbf{S}_i = -[\mathbf{A}_i]\nabla F(\mathbf{X}_i), \quad \mathbf{Y} = \nabla F(\mathbf{X}_{i+1}) - \nabla F(\mathbf{X}_i) \\ \mathbf{Z} = [\mathbf{A}_i]\mathbf{Y}, \quad [\mathbf{A}_{i+1}] = [\mathbf{A}_i] + \frac{\Delta\mathbf{X}\Delta\mathbf{X}^T}{\Delta\mathbf{X}^T\mathbf{Y}} - \frac{\mathbf{Z}\mathbf{Z}^T}{\mathbf{Y}^T\mathbf{Z}} \end{aligned}\right\}. \tag{3}$$

4) BFGS Method: The Broydon–Fletcher–Goldfarb–Shanno (BFGS) method is another VM method, whose metric is updated according to (4) and converges to the Hessian of the objective function as the solution is approached

$$\left.\begin{aligned} \mathbf{S}_i = -[\mathbf{A}_i]\nabla F(\mathbf{X}_i), \quad \mathbf{Y} = \nabla F(\mathbf{X}_{i+1}) - \nabla F(\mathbf{X}_i) \\ [\mathbf{A}_{i+1}] = [\mathbf{A}_i] + \frac{\mathbf{Y}\mathbf{Y}^T}{\mathbf{Y}^T\Delta\mathbf{X}} - \frac{\nabla F(\mathbf{X}_i)\nabla F(\mathbf{X}_i)^T}{\nabla F(\mathbf{X}_i)^T\mathbf{S}_i} \end{aligned}\right\}. \tag{4}$$

5) Pattern Search Method: In this nongradient optimization method, the search direction is cycled through the number of n variables in sequence and the $n+1$ search direction is assembled as a linear combination of the previous n search directions according to

$$\mathbf{S}_i = \sum_{j=1}^{n} \alpha_j \hat{\mathbf{e}}_j \tag{5}$$

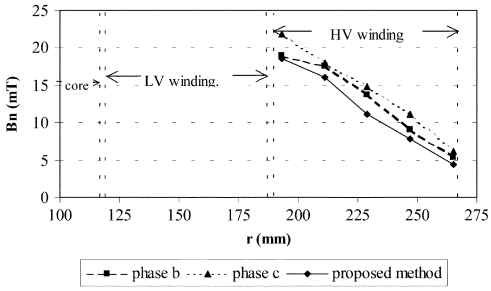

Fig. 2. Comparison of measured and computed field values along the line AB of Fig. 1 during short circuit.

TABLE I
SHORT-CIRCUIT IMPEDANCE VALUE FOR DIFFERENT GEOMETRY OF MAGNETIC SHUNT ON A 400 KVA, 20–15 KV/400 V TRANSFORMER

Geometry of magnetic shunt	U_k (%)	
	Coarse mesh	Dense mesh
Initial value (no shunt)	7.43	6.75
Magnetic shunt on the tank wall near the HV winding	7.60	6.92
Magnetic shunt on the tank walls near the HV winding and above the iron cores	7.71	7.02

IV. Results and Discussion

In order to investigate the accuracy of the proposed hybrid method for this class of problems, the computed field has been compared to the measured one by a Hall effect probe during short-circuit test. Fig. 2 gives the variation of the perpendicular flux density component B_n along the line AB, positioned as shown in Fig. 1, for a 400-kVA, rated primary voltage 20 and 15 kV (dual voltage in primary winding), rated secondary voltage 400-V, three-phase, wound core, power transformer in case of short circuit. The figure illustrates the good correlation of the simulated results with the local leakage field measurements, enabling application of the method in geometry optimization.

A. Formulation of the Objective Function

In order to evaluate the most effective shunt configuration, the short-circuit impedance has been calculated before and after the placement of shunts above and beside the transformer active part. Table I presents the simulated short-circuit impedance (U_k) by using a coarse and a dense mesh (comprising 2000 and 90 000 nodes, respectively). The short-circuit impedance is overestimated approximately 10%, when a coarse mesh is used, a difference relying on the fact that, with the use of this mesh, the magnetic filed sources (coils) area is not represented in detail, resulting to respective overestimation of the current density and the calculated U_k. The overestimation is practically constant for all three cases in Table I, as the active part mesh is the same and the sparsity of the mesh in the coils region affects the results in the same way.

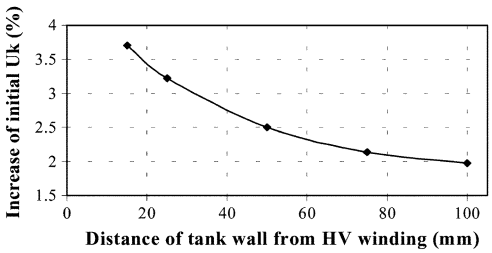

Fig. 3. Short-circuit impedance variation with the distance of magnetic shunt placed on the tank wall.

The results of Table I indicate that the geometry of the shunt near the HV coil is the one influencing the most the U_k variation. An investigation of the influence on U_k of the shunt distance from HV winding for this type of shunt has also been conducted, and the respective results are shown in Fig. 3. During this investigation, the shunt area was considered to be equal to the surface of the respective tank wall.

According to Fig. 3, an increase from 2% up to 4% can be achieved by approaching accordingly the shunt to the external HV coil surface. However, in such a case, the increase in the shunt power loss must be considered, since, as the distance from the windings decreases, the eddy current losses in the shunt increase, resulting to significant rise in the total transformer power loss. Moreover, changes in the shunt geometry (with respect to its distance from the windings) may produce different results in the U_k increase, thus optimizing the total shunt material needed for the achievement of the objective variation in the short-circuit impedance. Therefore, the search for the optimal configuration of the magnetic shunt becomes a complex task, taking into account variations of three variables, namely, the shunt width, height, and distance from HV winding. This is solved as a nonlinear, multicriteria, constrained optimization problem.

The objective function must take into account the three factors mentioned above: desired increase in short-circuit impedance, restrain of the increase in the shunt power loss and minimization of the shunt material. During the optimization process, the objective function value is calculated with the use of the hybrid FEM-BEM method described in Section II and a dense mesh (see Fig. 4). The analytical expression of the objective function is given by

$$F = w_1 \frac{\left|\mathrm{DU}_k^{\mathrm{calc}} - \mathrm{DU}_k^{\mathrm{spec}}\right|}{\mathrm{DU}_k^{\mathrm{spec}}} + w_2 \left|\frac{\mathrm{DP}_{\mathrm{shunt}}^{\mathrm{calc}}}{\mathrm{DP}_{\mathrm{shunt}}^{\mathrm{max}}}\right| + w_3 \frac{\mathbf{S}_{\mathrm{shunt}}^{\mathrm{calc}}}{\mathbf{S}_{\mathrm{shunt}}^{\mathrm{max}}} \quad (6)$$

where

$\mathrm{DU}_k^{\mathrm{calc}}$ calculated increase in the short-circuit impedance;
$\mathrm{DU}_k^{\mathrm{spec}}$ specified (desired) increase in U_k;
$\mathrm{DP}_{\mathrm{shunt}}^{\mathrm{calc}}$ calculated increase in the shunt power loss (compared to the shunt power loss for the maximum distance from the transformer windings);
$\mathrm{DP}_{\mathrm{shunt}}^{\mathrm{max}}$ maximum permissible increase in the shunt loss;
$\mathbf{S}_{\mathrm{shunt}}^{\mathrm{calc}}$ shunt surface used during the current iteration;
$\mathbf{S}_{\mathrm{shunt}}^{\mathrm{max}}$ maximum shunt surface;
w_1, w_2, w_3 weight coefficients of the objective function components.

A physical interpretation of the multiobjective function weights is that they should be proportional to the cost impact of the respective objective function components. This penalty approach was preferred from other stochastic methods, such as evolutionary algorithms, due to the larger number of function evaluations required by the latter ones. This fact has a great impact in the computational efficiency when considering objective function evaluations based on numerical techniques, especially in cases of 3-D configurations [11].

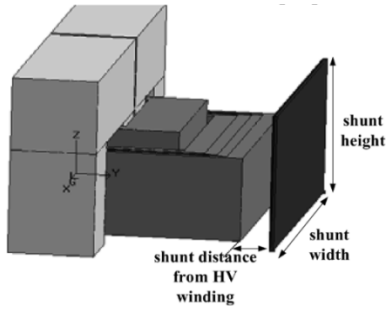

Fig. 4. Geometry of magnetic shunt configuration and design variables.

TABLE II
RESULTS OF DIFFERENT OPTIMIZATION METHODS (SPECIFIED $\mathrm{DUk} = 4\%$)

Method	*Optimal Shunt Geometry*			*Shunt Distance from HV coil (mm)*	DU_k^{calc} *(%)*	DP_{shunt}^{calc} *(%)*	*No of Iterations*
	Width (mm)	*Height (mm)*	*Total Area (mm^2)*				
Steep. Descent	350.00	68.3	23904	5.89	4.00	129.86	12
CG-FR	342.46	58.1	19909	0.43	4.00	137.05	11
DFP	349.99	57.7	20192	1.09	3.98	121.58	20
BFGS	350.00	56.1	19643	0.19	4.00	121.58	34
Pat.Search	350.00	86.9	30403	10.08	4.00	141.73	5

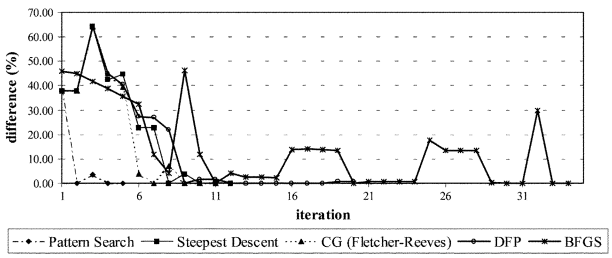

Fig. 5. Convergence to the target U_k value of the optimization methods illustrated in Table II.

B. Comparison of Different Optimization Methods

The methods presented in Section III.B were used to minimize the objective function (6) in case of $\mathrm{DU}_k^{\mathrm{spec}} = 4\%, \mathrm{DP}_{\mathrm{shunt}}^{\mathrm{max}} = 100\%$, and $\mathbf{S}_{\mathrm{shunt}}^{\mathrm{max}} = 60\,000$ mm^2. Table II summarizes the respective results for the optimal shunt geometry, the calculated increase in the short-circuit impedance and the shunt power loss (corresponding to the optimal solution given by each method) and the number of iterations needed for the convergence of each method. Fig. 5 illustrates the variation of the difference between the specified and calculated increase in U_k with the iterations of the methods of Table II.

The observation of the results listed in Table II and the curves of Fig. 5 leads to the following conclusions.

1) The pattern search is the quickest converging method, providing the optimal solution in the smallest number of iterations. However, this solution is inferior to the ones

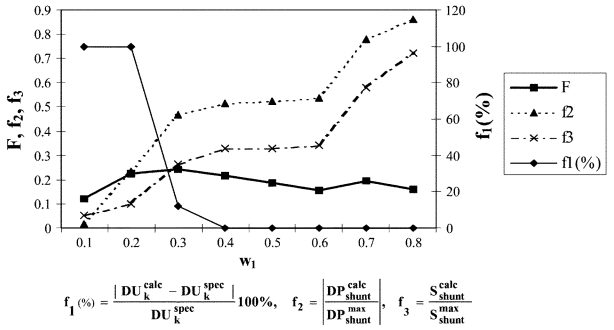

Fig. 6. Sensitivity of objective function and its components to the variation of weights coefficients.

provided by the gradient-based methods, as it corresponds to the greatest increase in the shunt power loss and area.

2) Between the gradient-based methods, the CG and the steepest descent are the ones concluding to the optimal solution in the least number of iterations. The CG solution is more effective in terms of construction cost, as it corresponds to the minimum total area.
3) The CG and BFGS methods converge practically to the same minimum, the only difference between them consisting in the total number of iterations.
4) Table II presents a significant variation between the optimal shunt height and distance from HV coil, through the different optimization methods. The CG-FR and BFGS methods result to the smaller distances (0.43 and 0.19 mm, respectively), which correspond to cases of shielding involving small optimum distance and reduced shield dimensions.

According to the above observations, the CG-FR method appears to be the most effective one for the solution of the magnetic shunt geometry optimization problem.

C. Sensitivity Analysis

A common difficulty with multiobjective optimization problem is the conflict between the objectives. In the optimization process of Section III, the weighted sum strategy was used, i.e., three objective functions were combined into the overall objective F such that

$$F(\mathbf{X}i) = \sum_{i=1}^{3} w_i f_i(\mathbf{X}i), \quad 0 \leqslant wi \leqslant 1, \qquad \sum_{i=1}^{3} w_i = 1. \quad (7)$$

For the selection of the appropriate weight vector w_i and the optimal scaling of each objective function component, a sensitivity analysis was carried out, with the use of CG-FR, i.e., the most effective of the methods presented in Section IV-B. A parametric investigation was realized, examining the impact of the weighting factor w_1 alteration to the variation of F and its components $f_1(\%), f_2$, and f_3 for different values of w_2 (w_3 is dependent on w_1 and w_2 according to (7)). Fig. 6 illustrates this variation for $w_2 = 0.1$. According to the diagram of Fig. 6, the objective function local minima appear for $w_1 = 0.1, 0.6$, and 0.8. However, for $w_1 = 0.1$, the deviation from the specified increase in U_k is close to 100%, while the shunt loss and area ratios are low enough to minimize the overall objective function. For values of w_1 above 0.3, the desired increase in the short-circuit impedance is achieved with acceptable tolerances in the two other objective function components, while for w_1 >0.6 the components f_2 and f_3 increase significantly. The extraction of the curves of Fig. 6 for greater values of w_2 produces local minimum values of F greater than the one appearing for $w_2 = 0.1$. Consequently, the choice of a weight coefficient vector equal to (0.6, 0.1, 0.3) is considered the most appropriate. This result has been confirmed through repetition of the above analysis with plots of F, f_1, f_2, and f_3 sensitivity to the alteration of w_2 and w_3.

V. Conclusion

This paper introduced the application of a 3-D mixed FEM-BEM method, based on a particular scalar potential formulation, to the geometry optimization of magnetic shunts on power transformers. The problem was solved as a nonlinear, multiobjective, constrained optimization problem and the proposed method was combined to several deterministic optimization algorithms. The CG-FR algorithm showed the best results in terms of convergence rate and optimal solution quality. For the optimal scaling of the multiple objectives considered, a sensitivity analysis was carried out, resulting to the appropriate formulation of the compound objective function.

Acknowledgment

This work was suppored in part by the General Secretariat for Research and Technology of Greece under PAVET Grant 00BE457.

References

[1] J. A. Ramirez, E. M. Freeman, C. Chat-Uthai, and D. A. Lowther, "Sensitivity analysis for the automatic shape design of electromagnetic devices in 3-D using FEM," *IEEE Trans. Magn.*, vol. 33, no. 2, pp. 1856–1859, Mar. 1997.
[2] J. M. Biedinger and D. Lemoine, "Shape sensitivity analysis of magnetic forces," *IEEE Trans. Magn.*, vol. 33, no. 3, pp. 2309–2316, May 1997.
[3] C. S. Koh, O. A. Mohammed, and S.-Y. Hahn, "Nonlinear shape design sensitivity analysis of magnetostatic problems using boundary element method," *IEEE Trans. Magn.*, vol. 31, no. 3, pp. 1944–1947, May 1995.
[4] *Power Transformers—Part 1: General*, IEC Standard 60 076-1, 2000.
[5] J. C. Olivares, Y. Liu, J. M. Canedo, R. Escarela-Perez, J. Driesen, and P. Moreno, "Reducing losses in distribution transformers," *IEEE Trans. Power. Del.*, vol. 18, no. 3, pp. 821–826, Jul. 2003.
[6] N. Takahashi, T. Kitamura, M. Horii, and J. Takehara, "Optimal design of tank shield model of transformer," *IEEE Trans. Magn.*, vol. 36, no. 4, pp. 1089–1093, Jul. 2000.
[7] M. Horii and N. Takahashi, "3D optimization of design variables in x-, y-, and z- directions of transformer tank shield model," *IEEE Trans. Magn.*, vol. 37, no. 5, pp. 3631–3634, Sep. 2001.
[8] M. A. Tsili, A. G. Kladas, P. S. Georgilakis, A. T. Souflaris, C. P. Pitisilis, J. A. Bakopoulos, and D. G. Paparigas, "Hybrid numerical techniques for power transformer modeling: A comparative analysis validated by measurements," *IEEE Trans. Magn.*, vol. 40, no. 2, pp. 842–845, Mar. 2004.
[9] A. Kladas and J. Tegopoulos, "A new scalar potential formulation for 3-D magnetostatics necessitating no source field calculation," *IEEE Trans. Magn.*, vol. 28, no. 4, pp. 1103–1106, 1992.
[10] P. Venkataraman, *Applied optimization with MATLAB programming*. New York: Wiley, 2002.
[11] K. Hameyer and R. Belmans, *Numerical Modeling and Design of Electrical Machines and Drives*. Southampton, U.K.: WIT Press, 1999.

Manuscript received June 8, 2004.